

GSH-Depleted PtCu₃ Nanocages for Chemodynamic-Enhanced Sonodynamic Cancer Therapy

Xiaoyan Zhong, Xianwen Wang, Liang Cheng,* Yong'an Tang, Guiting Zhan, Fei Gong, Rui Zhang, Jun Hu,* Zhuang Liu, and Xiangliang Yang*

The ultrahigh concentration of glutathione (GSH) inside tumors destroys reactive oxygen species (ROS)-based therapy, improving the outcome of chemodynamic therapy (CDT)-enhanced sonodynamic therapy (SDT) by depleting GSH is full of great challenge. Herein, PtCu₃ nanocages are first reported as acting as a sonosensitizer with highly efficient ROS generation under ultrasound irradiation. In addition, PtCu₃ nanocages can act as horseradish peroxidase-like nanozymes, catalyzing the decomposition of H₂O₂ into [•]OH under acidic conditions for CDT. Surprisingly, PtCu₃ nanocages can act as another kind of nanozyme, mimicking glutathione peroxidase (GSH-Px), which plays an important role in accelerating GSH depletion by oxidizing molecules, further weakening the capacity of tumor cells scavenging ROS by GSH. Both *in vitro* and *in vivo* studies demonstrate that PtCu₃ nanocages perform well in reducing GSH level for CDT-enhanced SDT. Moreover, utilizing the high absorption in the near-infrared region and strong X-ray attenuation ability, the PtCu₃ nanocages are able to conduct photoacoustic/computed tomography dual-modal imaging-guided combined cancer therapy. It is worth mentioning that PtCu₃ nanocages cause minimal toxicity to normal tissues at therapeutic doses. This work highlights the use of PtCu₃ nanocages for effective CDT-enhanced SDT via GSH depletion.

1. Introduction


Cancer continues to be one of the major global public health issues and the second leading cause of death in the world.^[1] To address this growing burden and achieve better therapeutics against cancer, many newly developed methods appear in addition to currently main treatments of surgery, chemotherapy, and radiotherapy.^[2–7] Reactive oxygen species (ROS)-based cancer therapy modalities with high toxicity have been widely applied in cancer therapy.^[8,9] Well-developed photodynamic therapy (PDT) as this kind of treatment can generate ROS by photosensitizers excited by UV–vis–NIR light.^[9] However, the limited penetration depth severely restricts the extensive PDT application, especially in deep-seated cancer therapy.^[10] The recently developed sonodynamic therapy (SDT), based on sonosensitizers triggered by the ultrasound (US) to generate highly toxic ROS, has emerged as a newly arisen noninvasive therapeutic modality.^[11–15] The US is a

type of mechanical wave with the advantage of high penetration up to ≈10 cm away from the skin, showing great potential to treat the deep-seated tumors without obstacle.^[15] However, the efficacy of SDT is still weakened by the complex tumor microenvironment (TME). TME is known as a complicated internal environment for the occurrence and development of tumors.^[16] Nevertheless, it is also utilized as an entrance for specific and efficient treatments of cancer. A groundswell of researches have been reported to regulate these various characteristics such as hypoxia, acidity, overexpressed hydrogen peroxide (H₂O₂), and others of tumors.^[17–20] Chemodynamic therapy (CDT) emerges as another kind of ROS-based therapeutic modality, by cleverly exploiting the two features of acidity and overexpressed H₂O₂ of TME. Through Fenton or Fenton-like reaction, highly toxic hydroxyl radicals ([•]OH) can be *in situ* generated by catalyzing H₂O₂ in acidic condition without external stimulus, avoiding the limited penetration issues and side effect to the healthy tissues.^[21] Therefore, both SDT and CDT preponderate in treating deep-seated tumors than PDT due to either the deep penetrating or circumventing aforementioned limitation by *in situ* generating ROS against cancers.

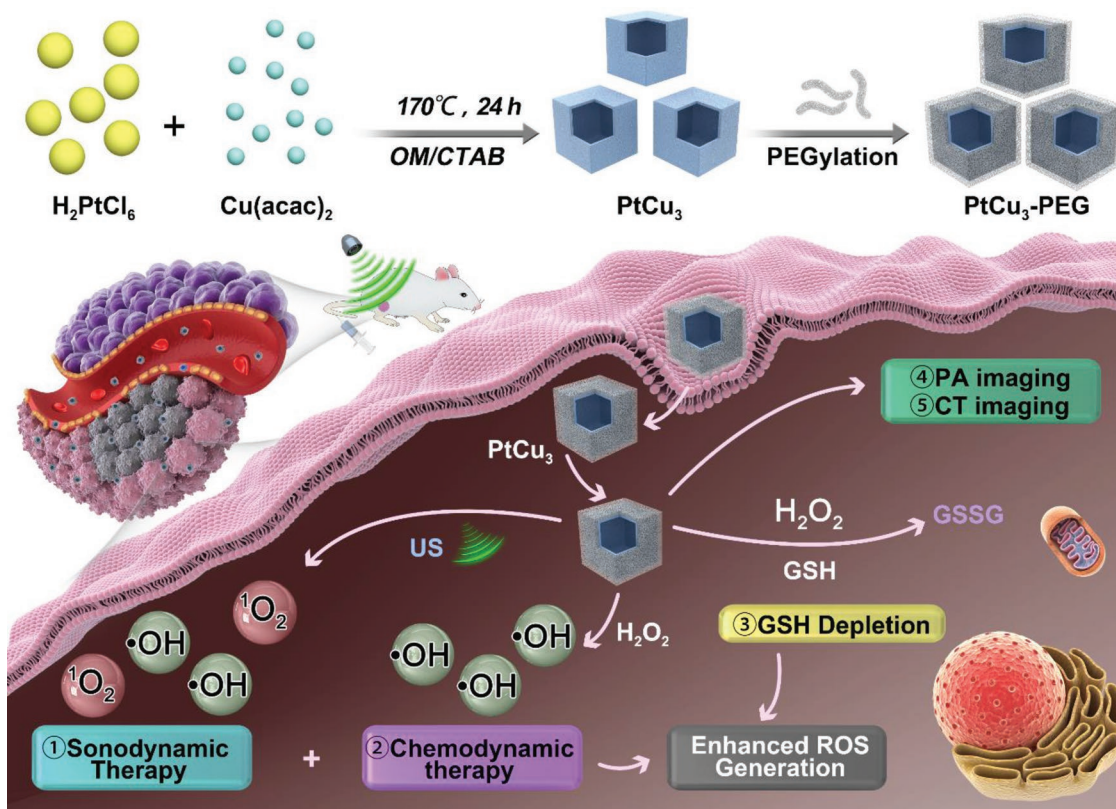
X. Zhong, G. Zhan, Prof. J. Hu, Prof. X. Yang
National Engineering Research Center for Nanomedicine
College of Life Science and Technology
Huazhong University of Science and Technology
Wuhan 430074, P. R. China
E-mail: hjun0718@hust.edu.cn; yangxl@hust.edu.cn

X. Wang, Prof. L. Cheng, F. Gong, R. Zhang, Prof. Z. Liu
Institute of Functional Nano and Soft Materials (FUNSOM)
Jiangsu Key Laboratory for Carbon-Based Functional Materials
and Devices
Soochow University
Suzhou 215123, P. R. China
E-mail: lcheng2@suda.edu.cn

Dr. Y. Tang
Collaborative Innovation Center for Optoelectronic Science
and Technology
Key Laboratory of Optoelectronic Devices and Systems
of Ministry of Education and Guangdong Province
College of Optoelectronic Engineering
Shenzhen University
Shenzhen 518060, P. R. China

 The ORCID identification number(s) for the author(s) of this article can be found under <https://doi.org/10.1002/adfm.201907954>.

DOI: 10.1002/adfm.201907954



Scheme 1. Schematic illustration of photoacoustic (PA)/computed tomography (CT) dual-modal imaging guided cancer chemodynamic therapy (CDT) and GSH depletion enhanced sonodynamic therapy (SDT) by PtCu₃ nanocages. The PtCu₃ nanocages as a new kind of sonosensitizer can generate singlet oxygen radical (¹O₂) and hydroxyl radical (•OH) under the US irradiation for SDT. In addition, PtCu₃ nanocages as horseradish peroxidase (HRP) mimic can generate •OH via Fenton-like reaction for CDT. Interestingly, PtCu₃ nanocages as another glutathione peroxidase (GSH-Px)-like nanozyme can accelerate the progress of GSH depletion by H₂O₂ to inhibit ROS scavenging by GSH for CDT-enhanced SDT.

Another feature, glutathione (GSH), in the form of intracellular free thiols, accounts for the majority of reductive small molecules in cells to generate highly reductive TME and functions in protecting cells from free radical induced oxidative damage.^[22] As a result, the therapeutic efficacies of ROS-based treatments will be largely compromised if GSH cannot be depleted timely. At present, several strategies have been explored to reduce GSH level inside tumor. For example, L-buthionine sulfoximine (BSO), an inhibitor of γ -glutamylcysteine synthetase, was utilized to inhibit the synthesis of GSH from the upstream pathways.^[23–25] Another strategy is converting the generated GSH to glutathione disulfide (GSSG) by oxidizers via redox reactions.^[26–28] Besides these two conventional methods, glutathione peroxidase (GSH-Px) with GSH as reductant has been known to catalyze the reduction of hydroperoxide.^[29] In this process, GSH can be depleted to GSSG by the oxidation of H₂O₂.^[30] Therefore, depleting GSH to simultaneously improve the efficacies of ROS-based treatments is of great importance.

Copper-based nanomaterials play essential roles in ROS-based cancer treatments.^[28,31,32] In particular, divalent copper ion (Cu²⁺) can deplete GSH through redox reaction and cuprous ion (Cu⁺) has been reported as highly efficient Fenton-like reagent.^[33] Nevertheless, simultaneously integrating CDT and GSH depletion to enhance SDT by a single system has not been reported

yet. Herein, PtCu₃ nanocages as a kind of copper-based nanomaterials are supposed to realize CDT-enhanced SDT in the manner of GSH-depletion (Scheme 1). Uniform PtCu₃ nanocages are synthesized via one-pot solvothermal method. After PEGylation, the synthesized PtCu₃-PEG nanocages not only function as a new kind of sonosensitizer to generate ROS under the US irradiation, including singlet oxygen (¹O₂) and •OH, but also serve as a horseradish peroxidase (HRP)-like nanozyme to catalyze the decomposition of H₂O₂ into •OH, a kind of cell killing ROS. Most importantly, the PtCu₃-PEG nanocages as another glutathione peroxidase (GSH-Px) nanozyme can accelerate the progress of GSH depletion in the presence of oxidizing molecules (H₂O₂, O₂). In vitro and in vivo studies confirm that higher sonotoxicity and delayed tumor growth can be achieved by PtCu₃-PEG nanocages via CDT-enhanced SDT due to the highly generated ROS and the sharply reduced GSH. In addition, utilizing the high optical absorption in the NIR region and strong X-ray attenuation capability, the PtCu₃-PEG nanocages can also conduct photoacoustic (PA)/computed tomography (CT) dual-modal imaging-guided CDT-enhanced SDT. No obvious toxicity of the synthesized PtCu₃-PEG nanocages is found at the injected dose. Our work highlight that the synthesized PtCu₃ nanocages can integrate functions of sonosensitizer, nanozymes of HRP, and GSH-Px into a whole system, for imaging-guided TME-responsive cancer treatment.

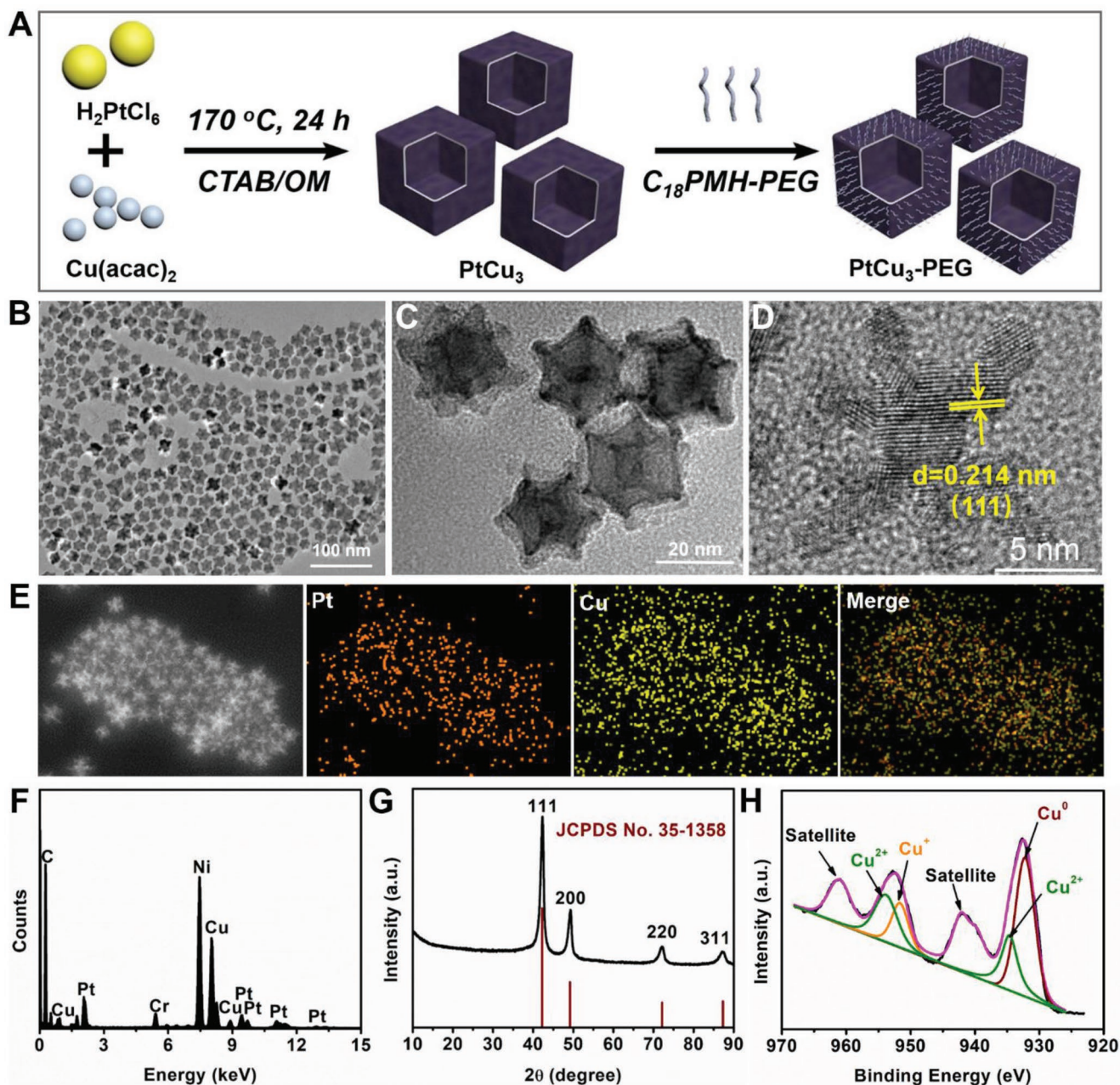


Figure 1. Synthesis and characterization of PtCu₃ nanocages. A) Schematic illustration of synthesis and modification of PtCu₃ nanocages. B,C) Low- and high-magnification transmission electron microscopy (TEM) images of PtCu₃ nanocages. D) High-resolution TEM (HRTEM) image of PtCu₃ nanocages. E,F) Scanning transmission electron microscopy-energy-dispersive spectrometer (STEM-EDS) elemental mapping analysis confirmed the coexistence of Pt and Cu in this structure. G) X-ray diffraction (XRD) of PtCu₃ nanocages. H) The surface valence status of Cu element in PtCu₃ nanocages provided by X-ray photoelectron spectroscopy (XPS).

2. Results and Discussion

PtCu₃ nanocages with cubic structure were synthesized using a simple solvothermal method according to the previous study (Figure 1A).^[34] X-ray diffraction (XRD) was first employed to characterize the crystalline structure. All the characteristic diffraction peaks were well indexed with the standard cubic PtCu₃ (JCPDS No. 35-1358) (Figure 1G). Transmission electron microscopy (TEM) image revealed the uniform morphology

of PtCu₃ with an average diameter of $\approx 14.29 \pm 2.78$ nm (Figure 1B; Figure S1, Supporting Information). From the high-magnification and high-angle annular dark field scanning TEM (HAADF-STEM) images, PtCu₃ nanocages with the cubic structure were exhibited clearly (Figure 1C; Figure S2, Supporting Information). In detail, high-resolution TEM (HRTEM) image confirmed the good crystallinity of PtCu₃ with an ordered fringe pattern and the lattice interval of 0.214 nm, which was agreed well with the (111) facet of PtCu₃

(Figure 1D; Figure S3, Supporting Information). Other high-index facets such as (200), (220), and (311) were also identified by selected area electron diffraction (SAED) pattern (Figure S3, Supporting Information). It was reported that such atomic structure as active sites could work for the highly catalytic reaction.^[35] X-ray energy-dispersive spectrometer (EDS) analysis and quantitation detection by inductively coupled plasma-optical emission spectrometry (ICP-OES) displayed the coexistence of Pt and Cu elements with the Pt/Cu molar ratio of $\approx 1:3$ (Figure 1E,F). Due to the polyvalency property of Cu element, X-ray photoelectron spectroscopy (XPS) spectrum of PtCu₃ nanocages was obtained (Figure S4, Supporting Information). The surface valence status of Cu element including the majority of Cu⁰, as well as Cu⁺ and Cu²⁺ (Figure 1H). This was probably due to the low redox potential of Cu⁺/Cu⁰ (≈ 0.52 V) and Cu²⁺/Cu⁺ (≈ 0.16 V), which resulted in the easy oxidation of partial Cu ions.^[27,33,36] For biomedical application, hydrophobic PtCu₃ nanocages were modified with poly (maleic anhydride-alt-1-octadecene)-polyethylene glycol (C₁₈PMH-PEG) through hydrophobic interaction to obtain water soluble PtCu₃-PEG.^[37] After surface coating, the hydrodynamic size of PtCu₃-PEG was measured to be ≈ 34 nm and the zeta potential was measured to be -6.28 mV (Figure S5, Supporting Information). The UV-vis-NIR spectra of the black colored PtCu₃-PEG nanocages showed the relatively high absorbance in the NIR region and good stability in physiological solution (Figures S6 and S7, Supporting Information).

The PtCu₃ nanocages as copper-based compounds with the arrangements of metal atoms highly ordered were supposed to act as a new type of sonosensitizer. To evaluate the properties of ROS generation under the US irradiation by PtCu₃-PEG nanocages, 1,3-diphenylisobenzofuran (DPBF) as a trapping agent of singlet oxygen (¹O₂) was first utilized to indicate the ability of ¹O₂ production. The US alone could attenuate $\approx 21.6\%$ of the DPBF probe, indicating a certain extent of ¹O₂ generation (Figure S8, Supporting Information). On the contrary, the color of DPBF probe was attenuated $\approx 71.7\%$ with PtCu₃-PEG under the US irradiation, indicating large amounts of ¹O₂ were generated (Figure 2A,B). In addition to ¹O₂, another kind of free radical, hydroxyl radical ([•]OH) was largely generated by PtCu₃-PEG under the US irradiation with *o*-phenylenediamine (OPD) as the trapping agent. Compared to the US alone, large amounts of [•]OH were generated by PtCu₃-PEG under the US irradiation (Figure 2D,E; Figure S9, Supporting Information). Apart from the colorimetric methods, electron spin resonance (ESR) with the spin traps of 2,2,6,6-tetramethylpiperidine (TEMP) and 5,5-dimethyl-1-pyrroline N-oxide (DMPO) were also applied to directly capture short-lived ¹O₂ and [•]OH, respectively. After being exposed to the US irradiation, the characteristic ¹O₂ (1:1:1) and [•]OH (1:2:2:1) signals could be clearly observed in PtCu₃-PEG solution (Figure 2C,F). It has been reported that Cu₂O as an excellent photosensitizer could generate ¹O₂ and [•]OH under light irradiation for PDT.^[38–40] To discuss the underlying mechanism of SDT mediated by PtCu₃-PEG nanocages, the SDT effect of Cu₂O nanoparticles was evaluated since the surface Cu ions contained Cu⁺ of PtCu₃-PEG. Under the US irradiation, both ¹O₂ and [•]OH could be generated with DPBF and OPD as the trapping agents, respectively (Figure S10,

Supporting Information). This indicated that the oxidized Cu ions in the form of Cu₂O afford PtCu₃-PEG a good property of generating ROS under the US irradiation.

Among ROS family including [•]OH, [•]O₂⁻, and ¹O₂, [•]OH is generally considered to be the most toxic one which can be produced through Fenton reaction in the presence of Fenton agents and H₂O₂ for CDT.^[8] Most importantly, the concentration of H₂O₂ in tumors is much higher (100×10^{-6} to 1×10^{-3} M) than normal tissues. Therefore, the [•]OH can be generated specifically in the tumor site while avoiding damage to the healthy tissue.^[8] To make sure that our PtCu₃-PEG nanocages characterized with high proportion of Cu⁺ could act as Fenton-like agent, 3,3',5,5'-tetramethylbenzidine (TMB) as the horseradish peroxidase (HRP) substrate with the existence of H₂O₂ was used here. With the elevated concentration of H₂O₂, the absorbance at 652 nm obviously increased with much deeper blue color, indicating more [•]OH generation in acidic buffer solution (pH 5.5), but limited in PBS (pH 7.4), promising in showing toxicity to tumor cells but healthy to normal cells (Figure 2G,H; Figure S11, Supporting Information). Moreover, ESR analysis further confirmed that PtCu₃-PEG nanocages and H₂O₂ alone generated negligible [•]OH, significant amplifying amounts of ROS was generated when PtCu₃-PEG nanocages meet with H₂O₂, which reflecting that PtCu₃-PEG nanocages with peroxidase-like activity could generate [•]OH in the presence of H₂O₂ (Figure 2F). This indicated that PtCu₃-PEG nanocages were indeed as a kind of good Fenton-like reagent for potential CDT.

Highly expressed GSH in tumor cells will decrease the efficacy of ROS-based treatments.^[41–43] We wondered whether the synthesized PtCu₃ nanocages had the ability for GSH depletion. The PtCu₃-PEG nanocages were incubated with excess GSH, the residual GSH was indicated by 5,5'-dithiobis (2-nitrobenzoic acid) (DTNB), a kind of sulphhydryl (–SH) indicator at different time points. With the extended time, the characteristic absorbance at ≈ 412 nm decreased, indicating the depletion of GSH (Figure 2I). To discuss the mechanism of depleting GSH by the PtCu₃ nanocages, the valence states of Cu ions in PtCu₃-PEG nanocages after incubation with GSH were analyzed. The proportion of Cu⁰ increased by the reduction of excess GSH (Figure S12, Supporting Information). This demonstrated that PtCu₃-PEG nanocages acting as an oxidizing agent could efficiently deplete GSH. However, PtCu₃-PEG nanocages could not completely oxidize GSH with the molar ratio of GSH to PtCu₃-PEG up to 10. Then, another control experiment was conducted to find out the leading role in GSH depletion. The GSH solution was bubbled with nitrogen to exclude oxygen (O₂) in advance; however, the GSH could not be depleted anymore (Figure S13, Supporting Information). These indicated that O₂ as the oxidizer played the major role in GSH depletion with PtCu₃-PEG as the catalyst. Considering the hypoxia microenvironment of tumors, H₂O₂ as another oxidizer with the oxidation capacity higher than O₂, was evaluated for GSH depletion. Upon adding H₂O₂ into this mixture, the GSH was rapidly depleted compared with PtCu₃-PEG nanocages and H₂O₂ alone (Figure 2J; Figure S14, Supporting Information). Here it should be noted that the fast depletion of GSH was not due to the generated [•]OH by PtCu₃-PEG upon adding 100×10^{-6} M of H₂O₂.

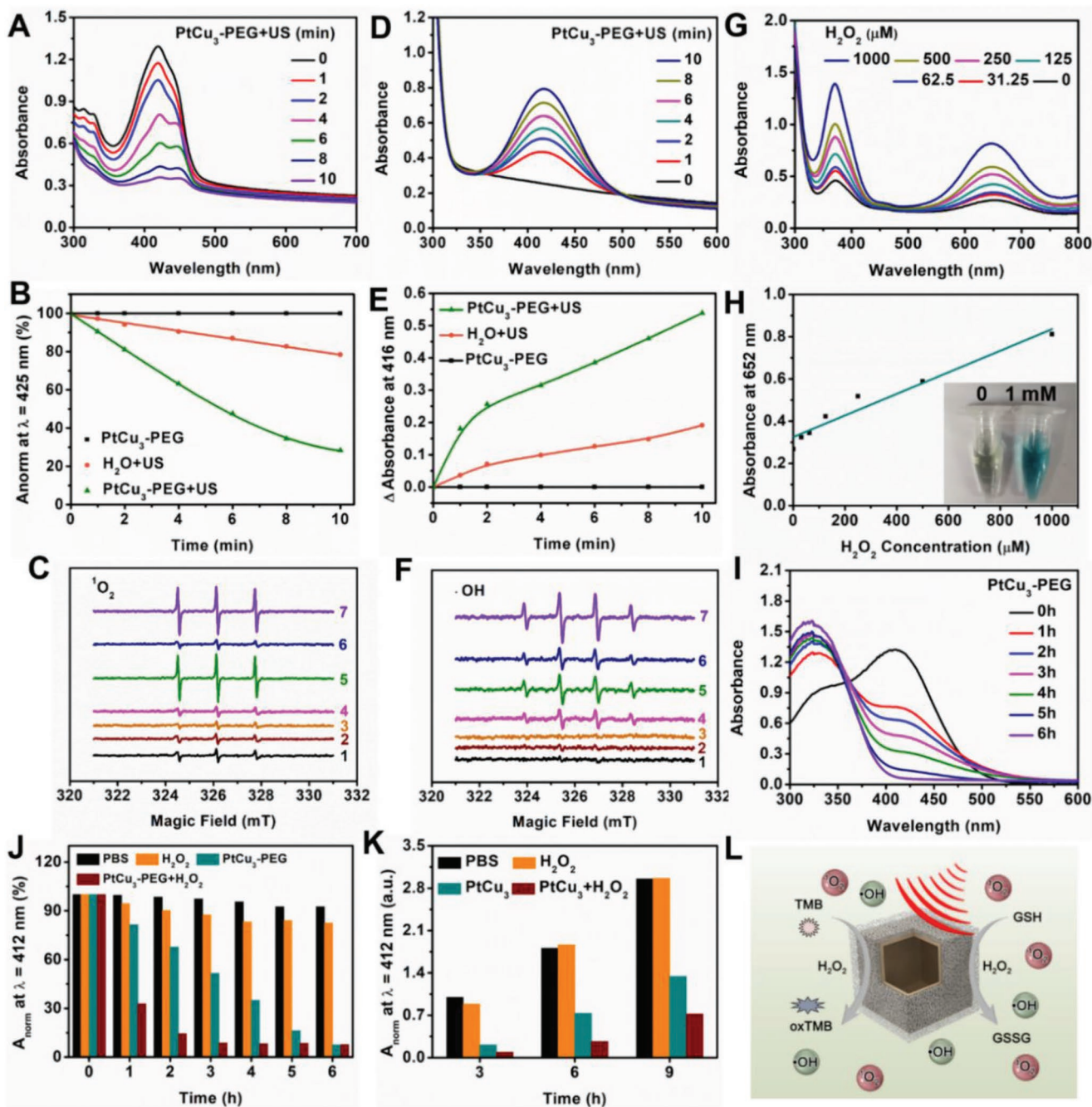
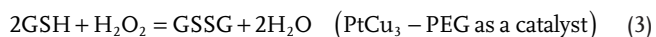
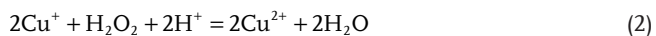
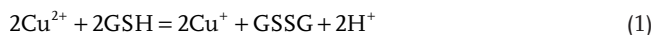


Figure 2. Properties of PtCu₃-PEG nanocages. A,B) Enhanced ¹O₂ generation of PtCu₃-PEG under the US irradiation with DPBF as the trapping agent. D,E) Enhanced ·OH generation of PtCu₃-PEG under the US irradiation with OPD as the trapping agent. C,F) ESR spectra of TEMP/¹O₂ and DMPO/·OH adducts in different solutions, respectively. The seven groups were 1) PtCu₃-PEG, 2) H₂O₂, 3) US, 4) PtCu₃-PEG + H₂O₂, 5) PtCu₃-PEG + US, 6) H₂O₂ + US, and 7) PtCu₃-PEG + H₂O₂ + US, respectively. The concentrations of both PtCu₃-PEG and H₂O₂ were 100 × 10⁻⁶ M and the US irradiation was 10 min (3 W cm⁻², 35 kHz). G,H) Peroxidase-like property of PtCu₃-PEG revealed by UV-vis spectra of HAC/NaAc buffer solution (pH 5.5) containing 100 × 10⁻⁶ M of PtCu₃-PEG and different concentrations of H₂O₂. I,J) GSH depleting abilities of different solutions with DTNB as the trapping agent of sulphhydryl (–SH) in GSH. K) Continuous depleting of GSH by PtCu₃-PEG in the presence of H₂O₂. GSH was repeatedly added at 3 and 6 h, respectively. L) The overall scheme showing mechanisms of ROS generations via Fenton-like reaction and the US irradiation with GSH depletion.

Negligible ·OH could be produced in alkaline PBS solution (pH 7.4) (Figure S11, Supporting Information). More interestingly, continuous depletion of GSH could also be realized by H₂O₂. With three cycles of adding GSH at 0, 3, and 6 h,

respectively, the dynamic depletion profile of GSH was monitored. It could be found that the GSH could be continuously depleted by PtCu₃-PEG nanocages in the presence of H₂O₂ (Figure 2K; Figure S15, Supporting Information). According

to the above analysis, the progress of depleting GSH was supposed to follow the two equations



Equation (3)^[30] is the superposition of Equations (1) and (2). Furthermore, by comparing the morphology and crystalline structure of PtCu₃-PEG nanocages before and after incubation with excess GSH, no change occurred as revealed by TEM and XRD results (Figure S16, Supporting Information). Finally, H₂O₂ played the leading role in depleting GSH with PtCu₃-PEG nanocages as the glutathione peroxidase (GSH-Px)-like nanozyme, which would be better for ROS-based treatments. Importantly, the Equation (1) could happen again for the circular reaction for GSH depletion (Figure S12, Supporting Information). Based on the above results, our PtCu₃-PEG nanocages could integrate several function of good sonosensitizer for SDT, excellent Fenton-like agent for CDT as well as special GSH-Px-like enzyme for GSH depletion into one system, promising for in vitro efficient cancer therapy (Figure 2L).

Inspired by the excellent properties of PtCu₃-PEG nanocages, in vitro CDT-enhanced SDT of 4T1 breast cancer cells were investigated. To evaluate the inherent CDT effect of PtCu₃-PEG, noncancerous human umbilical vein endothelial cells (HUVECs) and 4T1 cells were used due to the different levels of H₂O₂ inside cells.^[44] With different concentrations of PtCu₃-PEG nanocages, it showed no obvious cytotoxicity toward HUVECs even at 100 μg mL⁻¹, but an reduced viability of 4T1 cells was achieved (Figure 3A). Such a significantly different cytotoxicity profile indicated that in vitro CDT could be achieved. By further adding extra H₂O₂, an enhanced CDT of 4T1 cells happened much due to the highly generated ·OH (Figure 3B). For SDT assessment, 4T1 cells were incubated with PtCu₃-PEG nanocages with the maximum dose of 50 μg mL⁻¹, a dose did not induce any effect from CDT, followed by the US irradiation. Compared to the US alone, cell viabilities significantly decreased in a dose-dependent manner (Figure 3C). When combined with extra adding H₂O₂ and the US irradiation, the viability of 4T1 cells was significantly reduced (Figure 3D). The good performance of CDT-enhanced SDT was realized by PtCu₃-PEG nanocages. The above-mentioned catalysis of PtCu₃-PEG nanocages in GSH depletion motivated us to investigate intracellular GSH levels after different treatments. ThiolTracker Violet fluorescent dye was used for GSH visualization. GSH levels in PBS treated group showed bright green fluorescence, while the contents of GSH in SDT or CDT group were less than that in control group. When cells were concurrently treated with SDT and CDT, nearly no fluorescence could be observed (Figure 3E,G). Therefore, it indicated that GSH was indeed consumed by ROS generated via CDT and SDT.

To uncover the in vitro mechanism of PtCu₃-PEG nanocages for CDT and SDT, intracellular ROS levels were generally visualized by non-fluorescent 2',7'-dichlorofluorescein diacetate (DCFH-DA) probe, which could turn into fluorescent

2,7-dichlorofluorescein (DCF) in the case of ROS. Single treatment such as PtCu₃-PEG nanocages, H₂O₂, and the US only induced weak fluorescence intensities. Notably, PtCu₃-PEG nanocages under the US irradiation induced a large amount of ROS as revealed by the conspicuous green fluorescence in 4T1 cells. Further combined with H₂O₂, the intracellular ROS could be significantly improved (Figure 3F,H). As a result, the PtCu₃-PEG nanocages with the multiple properties of sonosensitizer, HRP-like as well as GSH-Px-like nanozymes could realize GSH depletion for CDT-enhanced SDT, promising in in vivo cancer therapy.

In addition to the high performance of ROS generations by PtCu₃-PEG nanocages, other intriguing properties included acting as contrast agents for multimodal imaging. Photoacoustic (PA) imaging as a noninvasive functional imaging modality is successively conducted to figure out penetration and retention effect of nanomaterials in vivo by using the high optical absorbance of light located in NIR range.^[45] Due to the high absorbance of PtCu₃-PEG nanocages in NIR region, much stronger PA signal appeared along with the increasing concentration of PtCu₃-PEG nanocages (Figure 4A). Confidently, female Balb/c mice bearing 4T1 tumors were intravenously administrated with PtCu₃-PEG nanocages followed by PA imaging. PA signal gradually increased and sustained in the tumor regions for at least 3 days, showing excellent performance of enhanced penetration and retention (EPR) effect (Figure 4C,E). For dynamic monitoring in vivo behavior of PtCu₃-PEG nanocages, they were labeled with Cyanine 5.5 (Cy 5.5) probe to conduct fluorescence imaging. PtCu₃-PEG nanocages could accumulate at tumor site for a long time, agreed well with the PA imaging result (Figure 4D; Figure S17, Supporting Information). In addition to fluorescence imaging, PtCu₃-PEG nanocages might act as CT imaging contrast agent benefiting from the strong X-ray attenuation ability of Pt. The slope of HU value was calculated to be ≈61.44 HU L g⁻¹, a little higher than that of commercially used Iohexol (56.73 HU L g⁻¹) (Figure 4B). After the local injection of PtCu₃-PEG nanocages, in vivo CT imaging also displayed brighten tumor site, and the HU value increased from ≈28 to ≈96 (Figure 4F). Quantitative biodistribution profile indicated that PtCu₃-PEG nanocages could efficiently accumulate in tumors after intravenous injection, with the retention efficiency up to 10.08 ± 0.07 %ID g⁻¹, which was high enough to guarantee the following cancer therapy (Figure S18, Supporting Information).

The high performance and good tumor accumulation of PtCu₃-PEG nanocages motivated us to conduct the in vivo therapeutic evaluation. Female Balb/c mice were randomly divided to six groups: 1) PBS, 2) PtCu₃-PEG, 3) US irradiation only for 5 min, 4) US irradiation only for 10 min, 5) PtCu₃-PEG + US irradiation for 5 min, and 6) PtCu₃-PEG + US irradiation for 10 min. The dosage of administration was 10 mg kg⁻¹, and the parameters of US irradiation were set to 3.0 W cm⁻², 35 kHz, and 1 min per cycle for ten cycles. The US transducer was placed 5 mm over 4T1 tumor (Figure S19, Supporting Information). The progress of US irradiation in each group of 3, 4, 5, and 6 was repeated three times for the consecutive 3 days (Figure 5A). Once started the treatment, the tumor volume and body weight of each mouse were monitored every 2 days. Rapid tumor growth appeared in PBS treated group, while PtCu₃-PEG

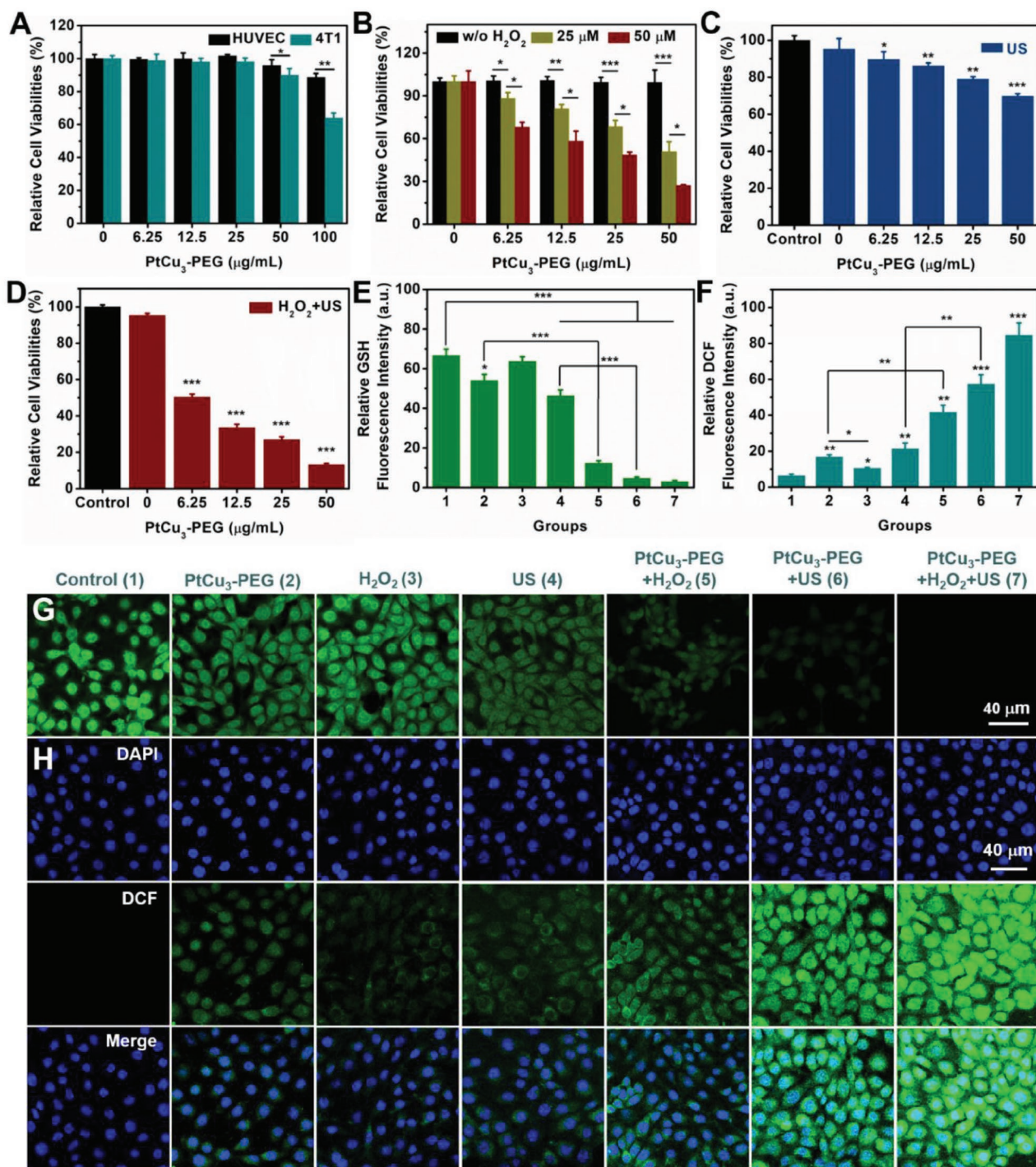


Figure 3. In vitro CDT and SDT effect of PtCu₃-PEG nanocages. A) Relative cell viabilities of HUVECs and 4T1 cells with different concentrations of PtCu₃-PEG. B) PtCu₃-PEG induced CDT by adding different concentrations of H₂O₂. C) PtCu₃-PEG induced SDT under the US irradiation in 4T1 cells. D) CDT-enhanced SDT of 4T1 cell. E,G) CLSM images and quantification of intracellular GSH in 4T1 cells with different treatments. GSH level was stained by ThiolTracker Violet (green). The seven groups were 1) control, 2) PtCu₃-PEG, 3) H₂O₂, 4) US, 5) PtCu₃-PEG + H₂O₂, 6) PtCu₃-PEG + US, and 7) PtCu₃-PEG + H₂O₂ + US. The concentrations of PtCu₃-PEG and H₂O₂ were 100 × 10⁻⁶ and 25 × 10⁻⁶ M. The US irradiation was 10 min (3 W cm⁻², 35 kHz). F,H) CLSM images and quantification of ROS generation in 4T1 cells with various treatments. The ROS inside cells were stained by DCFH-DA probe (**p* < 0.05, ***p* < 0.01, ****p* < 0.001).

nanocages and the US only led to moderate growth of tumors. On the contrary, tumors in mice simultaneously received PtCu₃-PEG nanocages and the US irradiation significantly

inhibited compared with other groups (Figure 5B). Notably, tumor growth in group 6 was much slower as compared to group 5, which might be benefited from large amount of ROS

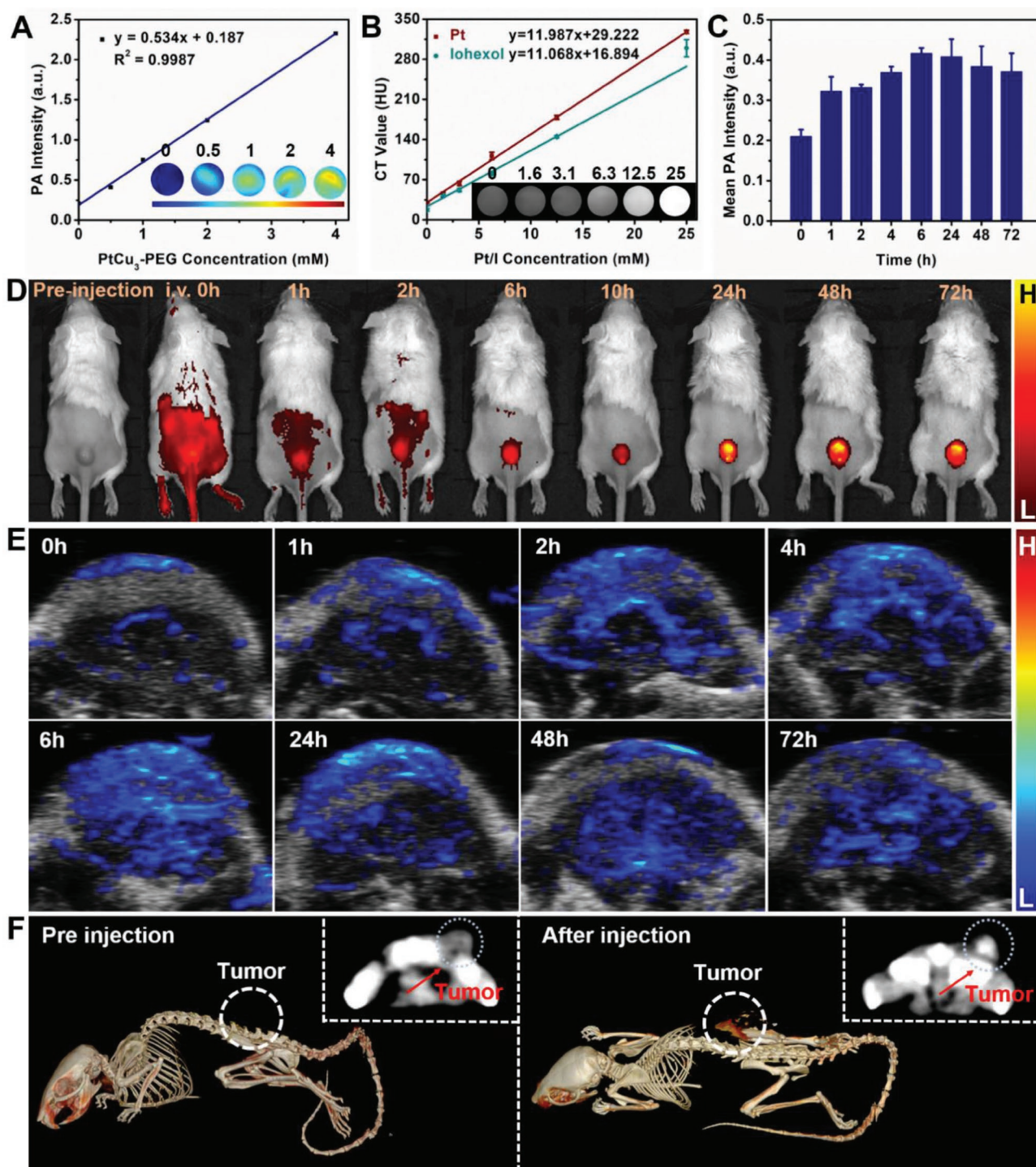


Figure 4. Multimodal imaging of PtCu₃-PEG nanocages. A) Photoacoustic (PA) imaging of PtCu₃-PEG solutions with different concentrations. B) CT imaging of PtCu₃-PEG solution and Iohexol with the same concentration. Increased concentrations of PtCu₃-PEG led to enhanced signals with brighter effect. D) Fluorescence imaging of 4T1 tumors by intravenous injection of Cy5.5-labeled PtCu₃-PEG. C, E) In vivo PA imaging of 4T1 tumors by intravenous injection of 10 mg kg⁻¹ of PtCu₃-PEG in (E) and the PA signals changed over time were analyzed in (C). F) In vivo CT imaging of tumor-bearing mouse by intratumorally injecting 10 mg kg⁻¹ of PtCu₃-PEG. The HU values of tumors increased from ≈28 to ≈96 with an obvious enhancement located at tumor sites.

generation due to the longer US irradiation time mediated by PtCu₃-PEG nanocages. From the above analysis, the performance of CDT-enhanced SDT had been successfully realized

(Figure 5C; Figure S20, Supporting Information). Additionally, hematoxylin and eosin (H&E) staining and TdT-mediated dUTP Nick-End Labeling (TUNEL) staining of tumor section further

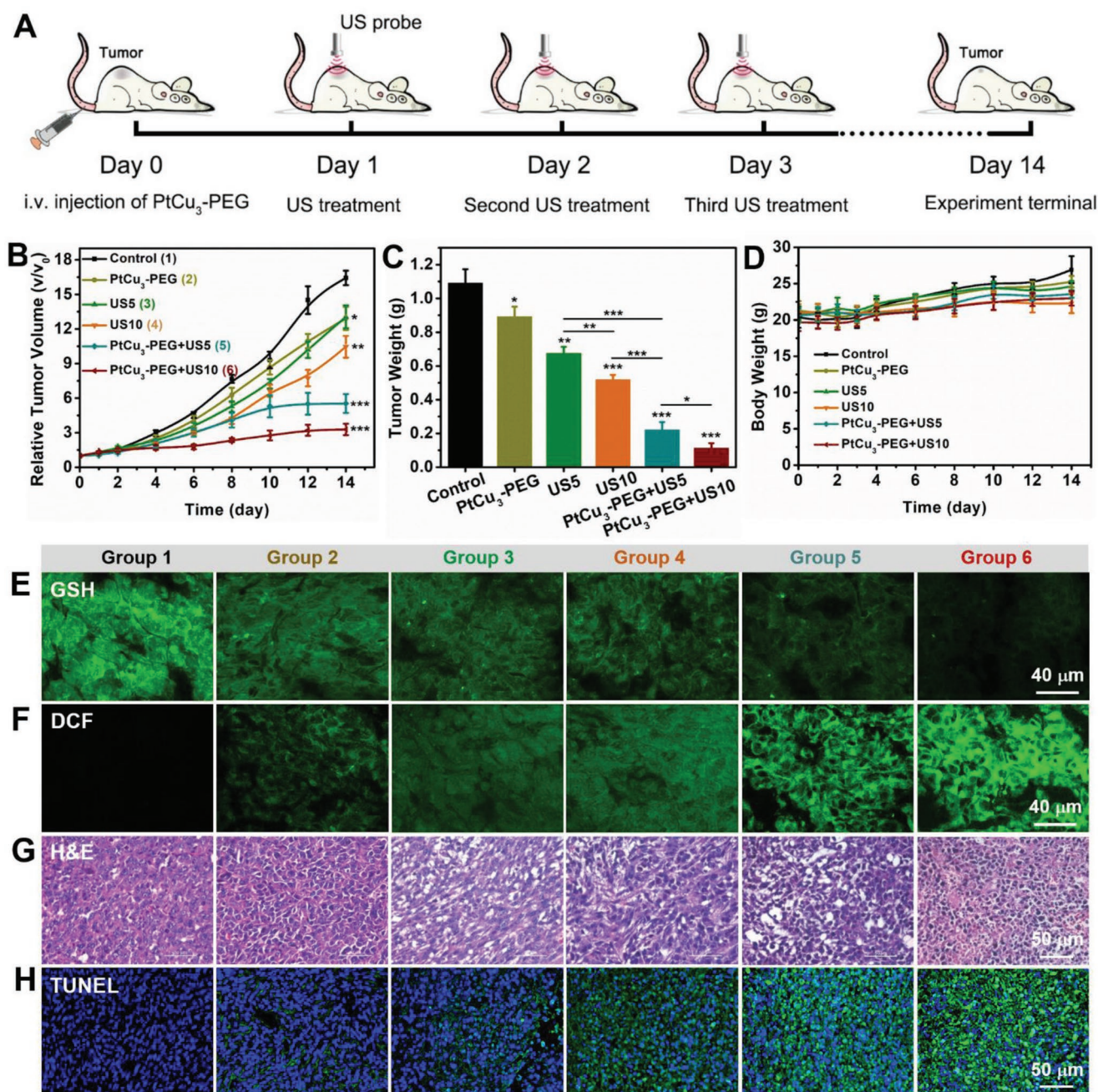


Figure 5. In vivo CDT-enhanced SDT of 4T1-bearing mice. A) Schematic illustration of treatment schedule for SDT mediated by PtCu₃-PEG in 4T1 tumor model. B) Tumor growth curves of mice received 1) PBS, 2) PtCu₃-PEG, 3) ultrasound irradiation for 5 min, 4) ultrasound irradiation for 10 min, 5) PtCu₃-PEG plus ultrasound irradiation for 5 min, and 6) PtCu₃-PEG plus ultrasound irradiation for 10 min. C) Tumor weights at the endpoint of treatment schedule. D) Body weights changes during the treatment with no body loss in each group. E-H) GSH, ROS, H&E, and TUNEL staining of tumors after three-round of treatments, respectively (**p* < 0.05, ***p* < 0.01, ****p* < 0.001).

confirmed that the tumor in group 6 showed severe apoptosis (Figure 5G,H). During the observation period, the body weights of mice in all groups showed increment, demonstrating the negligible adverse consequence of the injected dose of PtCu₃-PEG nanocages happened on mice (Figure 5D). After the treatment for 14 days, all of the major organs in the long-time US irradiation treated groups were well in morphologies compared with control group (Figure S21, Supporting Information).

In order to reveal the performance mechanism of PtCu₃-PEG nanocages, the tumors were collected at 6 h after different treatments for ROS and GSH staining. In vivo ROS was visualized by DCFH-DA probe. It was found that both CDT and the US could improve ROS levels, while higher level of that could be generated by CDT-enhanced SDT (Figure 5F). Meanwhile, high fluorescence intensity of GSH appeared in PBS treated group or relatively high fluorescence intensity appeared in PtCu₃-PEG

nanocages treated group. The US irradiation alone markedly attenuated the fluorescence intensity. Furthermore, nearly no fluorescence signal could be observed in CDT-enhanced SDT group (Figure 5E). The more GSH depletion, the higher ROS levels in tumors.

As biosafety of nanomaterials is a precondition for biomedical application, healthy female Balb/c mice were sacrificed after intravenous injection with 10 mg kg⁻¹ of PtCu₃-PEG nanocages for 1, 7, and 30 days, respectively. No significant changes occurred about blood routine indexes and liver and renal function induced by PtCu₃-PEG nanocages compared to the control group (Figures S22 and S23, Supporting Information). Additionally, H&E staining showed that no morphological change occurred (Figure S24, Supporting Information). Overall, the biosafety assessments pointed out that the synthesized PtCu₃-PEG nanocages were highly biocompatible, showing no apparent long-term toxicity.

3. Conclusions

In summary, the uniform PtCu₃ nanocages as a kind of novel sonosensitizer are simply prepared for multimodal imaging-guided SDT with high performance of generating ROS for cancer therapy. The PtCu₃ nanocages as multienzyme mimics can modulate TME to improve SDT efficacy. The PtCu₃ nanocages not only as HRP-like enzyme to generate [•]OH in the presence of H₂O₂ at acidic TME for CDT, but also act as another nanozyme of GSH-Px mimic to accelerate the progress of GSH depletion by oxidizing molecules (H₂O₂, O₂), inhibiting GSH induced ROS scavenging. In vitro and in vivo studies confirm the remarkable sonotoxicity enhanced by CDT and GSH depletion without any apparent side effect systematically. Combined with the intrinsic properties of PA/CT imaging, the intelligent PtCu₃ nanocages can pave a new way for imaging-guided in situ TME-responsive CDT-enhanced SDT triggered by the US irradiation for deep-seated tumors.

4. Experimental Section

Materials: Chloroplatinic acid solution (8 wt% H₂PtCl₆ in H₂O), 1,3-diphenylisobenzofuran (DPBF), 5,5-dimethyl-1-pyrroline N-oxide (DMPO, 97%), 2,2,6,6-tetramethylpiperidine (TEMP), 5,5'-dithiobis (2-nitrobenzoic acid) (DTNB) and 2',7'-dichlorofluorescein diacetate (DCFH-DA) were purchased from Sigma-Aldrich. Copper acetylacetonate (Cu(acac)₂, 98%) was purchased from Alfa Aesar. Cetyltrimethylammonium bromide (CTAB, 99.0%), polyvinylpyrrolidone (PVP K30, M_w = 40 000 Da), Copper chloride dehydrate (CuCl₂·2H₂O), sodium hydroxide (NaOH), and ascorbic acid (AA) were purchased from Sinopharm Chemical Reagent Co., Ltd. Oleylamine (OM, 80–90%) was obtained from Aladdin. ThiolTracker Violet (Glutathione Detection Reagent) was purchased from ThermoFisher Scientific. 3,3',5,5'-Tetramethylbenzidine (TMB) was purchased from Tokyo Chemical Industry Co., Ltd. (TCI, Shanghai, China). *o*-Phenylenediamine (OPD, 99.5%) was purchased from J&K Scientific. Fetal bovine serum (FBS), penicillin–streptomycin solution and RPMI-1640 medium were purchased from Gibco (Shanghai, China).

4T1 mouse breast cancer cell line was purchased from Cell Bank of Chinese Academy of Sciences (Shanghai, China). Female Balb/c mice were obtained from Nanjing Peng Sheng Biological Technology Co., Ltd. (Nanjing, China).

One-Pot Synthesis of PtCu₃ Nanocages: Cubic structured PtCu₃ nanocages were fabricated by a simple solvothermal method according to the previous report.^[34] In a typical synthesis, 131 mg of H₂PtCl₆ solution (8 wt% in H₂O) was added to 8 mL of oleylamine solution containing 20 mg of Cu(acac)₂ and 50 mg of cetyltrimethylammonium bromide (CTAB). The mixture was fully mixed by ultrasonication for 30 min. After that, the mixture was transferred to a 20 mL Teflon-lined autoclave and heated to 170 °C for 24 h. The product were collected by centrifugation and washed out with ethanol. The black precipitates were redispersed in chloroform at 4 °C for further use. In brief, 1 mL of C₁₈PMH-PEG solution (chloroform, 50 mg mL⁻¹) was dropwise added into 5 mL of PtCu₃ solution (chloroform, 1 mg mL⁻¹) under sonication. After sonication for 30 min, the solution was kept stirring at room temperature overnight. Finally, the solution was blown dry with nitrogen and then redispersed in DI water to obtain PtCu₃-PEG aqueous solution.

Synthesis of Cu₂O Nanoparticles: In a typical synthesis,^[44] 0.5 mmol of CuCl₂·2H₂O was dissolved in 20 mL of DI water at ambient conditions with 600 mg of polyvinylpyrrolidone (PVP) as a capping agent. Then 8 mmol of NaOH was dropwise added and stirred for 10 min, followed by adding 0.5 mmol of ascorbic acid to reduce Cu²⁺. After reaction for 10 min, the solution with orange color was collected and washed with DI water for several times. The concentrated Cu₂O nanoparticles were stored at 4 °C for the following studies.

PEG Modification of PtCu₃ Nanocages: Polyethylene glycol (PEG) grafted poly (maleic anhydride-alt-1-octadecene) (C₁₈PMH-PEG), which was synthesized according to the previous report, was used to modify PtCu₃ nanocages through hydrophobic interaction.^[26]

Characterization: Powder X-ray diffraction (XRD) measurement was carried out by PANalytical X-ray diffractometer equipped with Cu K α radiation ($\lambda = 0.15406$ nm). Transmission electron microscope (TEM) images and elemental mapping images were obtained by FEI Tecnai F20 TEM. X-ray photoelectron spectroscopy (XPS) analysis was performed by Thermo ESCALAB 250XI. Singlet oxygen (¹O₂) and hydroxyl radicals ([•]OH) were quantified by an electron spin resonance (ESR) spectrometer (Bruker EMXplus). UV–vis–NIR absorbance spectra were recorded by PerkinElmer Lambda 750 UV–vis–NIR spectrophotometer. The ultrasonic generator was made by Hainertec (Suzhou) Co., Ltd. The concentrations of Pt and Cu were detected by inductively coupled plasma optical emission spectrometry (ICP-OES).

ROS Generation under the Ultrasound: 50 × 10⁻⁶ M of PtCu₃-PEG was mixed with 20 μ g mL⁻¹ of DPBF (60 μ L, 1 mg mL⁻¹) in 3 mL of PBS. The mixture was under the US irradiation for 10 min (3 W cm⁻², 35 kHz). The UV–vis spectra of the samples were scanned to monitor the attenuation trend at 425 nm at different time points, which indicated the generation of singlet oxygen (¹O₂). Then, 50 × 10⁻⁶ M of PtCu₃-PEG was mixed with 1 × 10⁻³ M of OPD (20 μ L, 100 × 10⁻³ M) in 3 mL of PBS. The mixture was under the US irradiation for 10 min (3.0 W cm⁻², 35 kHz). The UV–vis spectra of the samples were scanned to monitor the ascending trend at 416 nm at different time points, which indicated the generation of [•]OH. The ROS generating ability of Cu₂O nanoparticles was conducted with the same methods.

Fenton-Like Reaction: 100 × 10⁻⁶ M of PtCu₃-PEG was incubated with different concentrations of H₂O₂ (0, 31.25, 62.5, 125, 250, 500, and 1000 × 10⁻⁶ M) in 2 mL of HAc/NaAc buffer solutions (pH 5.5) or PBS (pH 7.4), and TMB (20 μ L) was used as an indicator of [•]OH. Thirty minutes later, the UV–vis–NIR spectra of the samples were scanned to monitor the ascending trend at 652 nm, which indicated the generation of [•]OH.

ESR Measurements of ¹O₂ and [•]OH: For the measurements of ¹O₂ and [•]OH generated by PtCu₃-PEG under the US irradiation or H₂O₂, 25 × 10⁻³ M of BMPO and DMPO were used to detect ¹O₂ and [•]OH, respectively. The seven groups were 1) PtCu₃-PEG, 2) H₂O₂, 3) US, 4) PtCu₃-PEG + H₂O₂, 5) PtCu₃-PEG + US, 6) H₂O₂ + US, and 7) PtCu₃-PEG + H₂O₂ + US. The concentrations of both PtCu₃-PEG and H₂O₂ were 100 × 10⁻⁶ M and the US irradiation was 10 min (3 W cm⁻², 35 kHz).

GSH Depleting with PtCu₃-PEG: PBS, H₂O₂ (0.1 × 10⁻³ M), PtCu₃-PEG (0.1 × 10⁻³ M), and the mixture of 0.1 × 10⁻³ M H₂O₂ and 0.1 × 10⁻³ M of PtCu₃-PEG were mixed with 1 × 10⁻³ M of GSH solution in PBS solution

(pH 7.4) at room temperature, respectively. At different time points, 100 μL of mixture was pipetted and diluted to 900 μL of PBS followed by adding 0.2×10^{-3} M DTNB to detect $-\text{SH}$ of GSH. For discovering the continuously GSH depletion property of PtCu₃-PEG, 1×10^{-3} M of GSH was added again at 3 and 6 h to the above solutions, respectively. At different time points, 100 μL of mixture was pipetted and diluted to 900 μL of PBS followed by adding 0.2×10^{-3} M DTNB to detect $-\text{SH}$ of the residual GSH.

In Vitro CDT-Mediated by PtCu₃-PEG: Human umbilical vein endothelial cells (HUVECs) and 4T1 cells were seeded into 96-well plate at the density of 8×10^3 cells per well and incubated in 5% CO₂ at 37 °C until adherent, respectively. Cells were treated with different concentrations of PtCu₃-PEG for 24 h. Then, the cytotoxicity was determined with standard MTT assay.

In Vitro H₂O₂-Enhanced CDT-Mediated by PtCu₃-PEG: 4T1 cells were seeded into 96-well plate at the density of 8×10^3 cells per well and incubated in 5% CO₂ at 37 °C until adherent. Cells were treated with different concentrations of PtCu₃-PEG for 6 h. Then, cells were further incubated with 25×10^{-6} or 50×10^{-6} M of H₂O₂ and continuously incubated for 18 h, respectively. Then the cytotoxicity was determined with standard MTT assay.

In Vitro SDT-Mediated by PtCu₃-PEG: 4T1 cells were seeded into 24-well plate at the density of 8×10^3 cells per well and incubated in 5% CO₂ at 37 °C until adherent. Cells were treated with different concentrations of PtCu₃-PEG for 6 h. Then cells were exposed to the US (3.0 W cm^{-2} , 35 kHz, 1 min per cycle, ten cycles) for 10 min and continuously incubated for 18 h. The US induced cytotoxicity mediated by PtCu₃-PEG was also determined with standard MTT assay.

In Vitro CDT-Enhanced SDT Mediated by PtCu₃-PEG: 4T1 cells were seeded into 24-well plate at the density of 8×10^3 cells per well and incubated in 5% CO₂ at 37 °C until adherent. Cells were incubated with different concentrations of PtCu₃-PEG for 6 h. Then, cells were further incubated with 25×10^{-6} M of H₂O₂, followed by exposing to the US (3.0 W cm^{-2} , 35 kHz, 1 min per cycle, ten cycles) and continuously incubated for 18 h. Cytotoxicity of CDT-enhanced SDT mediated by PtCu₃-PEG was also determined with standard MTT assay.

In Vitro ROS Generations Mediated by PtCu₃-PEG: 4T1 cells were seeded into 35 mm confocal dish at the density of 2×10^5 cells and incubated in 5% CO₂ at 37 °C until adherence. Cells were exposed to different treatments including PBS, PtCu₃-PEG, H₂O₂ (25×10^{-6} M), US (3.0 W cm^{-2} , 35 kHz, 1 min per cycle, ten cycles), PtCu₃-PEG + H₂O₂, PtCu₃-PEG + US, and PtCu₃-PEG + H₂O₂ + US. Then, cells were incubated with DCFH-DA (20×10^{-6} M) followed by staining with DAPI. Different treatments induced ROS generations that were imaged with confocal laser scanning microscope (CLSM, Zeiss Axio-Imager LSM-800).

In Vivo Pharmacokinetics Studies: For Biodistribution study, female Balb/c mice were subcutaneously implanted with 2×10^6 tumor cells. When tumors reached to 60 mm³, tumor-bearing mice were intravenously injected with 10 mg kg⁻¹ of PtCu₃-PEG. 24 h later, tumors and vital organs of heart, liver, spleen, lung, and kidney were collected and weighted. The content of Pt in each sample was detected by inductively coupled plasma-optical emission spectrometry (ICP-OES).

In Vitro and In Vivo Multimodal Imaging with PtCu₃-PEG: For in vitro photoacoustic (PA) imaging, PtCu₃-PEG solutions with different concentrations ($0\text{--}4 \times 10^{-3}$ M) were imaged with the Visualsonic Vevo 2100 LAZER PA imaging system. For in vivo PA imaging, all animals were acclimated to the animal facility at least one week prior to experimental procedures. Female Balb/c mice were subcutaneously implanted with 2×10^6 tumor cells first. Tumor-bearing mice were administrated with 10 mg kg⁻¹ of PtCu₃-PEG nanocages, followed by tumor imaging with the Visualsonic Vevo 2100 LAZER PA imaging system at time points of 0, 1, 2, 4, 6, 24, 48, and 72 h. The dynamic change trends of PA signals located at tumor sites were analyzed.

For in vivo fluorescence imaging, tumor-bearing mice were intravenously injected with Cy5.5-labeled PtCu₃-PEG nanocages and imaged by Maestro EX in vivo optical imaging system (Cambridge Research and Instrumentation, Inc.) at time points of 0, 1, 2, 6, 10, 24,

48, and 72 h. The dynamic changes of fluorescence intensities located at tumor sites were analyzed.

For in vitro CT imaging, $(0\text{--}25) \times 10^{-3}$ M of PtCu₃-PEG and Iohexol solutions was scanned with CT imaging instrument, respectively. For in vivo CT imaging, tumor-bearing mice with or without intratumor-injecting 10 mg kg⁻¹ PtCu₃-PEG were scanned with CT imaging instrument (Hiscan In Vivo Micro-CT, Hiscan-H100), respectively.

In Vivo CDT-Enhanced SDT by PtCu₃-PEG: All animals were acclimated to the animal facility at least one week prior to experimental procedures. Balb/c female mice were subcutaneously implanted with 2×10^6 tumor cells first. When tumors reached to 60 mm³, tumor-bearing mice were randomly divided into six groups: 1) PBS, 2) PtCu₃-PEG, 3) US irradiation only for 5 min, 4) US irradiation only for 10 min, 5) PtCu₃-PEG + US irradiation for 5 min, and 6) PtCu₃-PEG + US irradiation for 10 min. In groups 2, 5, and 6, mice were intravenously injected with 10 mg kg⁻¹ PtCu₃-PEG. The parameters of US irradiation were set to 3.0 W cm^{-2} , 35 kHz, and 1 min per cycle for ten cycles for consecutive 3 days. After treatments, the volumes and weights of tumors were monitored every other day.

Histology Analysis of Tumor: For GSH staining, tumors were embedded in tissue freezing medium at -20 °C. After completely frozen, the tumor slices were fixed in acetone and washed with PBS. Then the tumor slices were incubated with ThiolTracker Violet dye (20×10^{-6} M) for 1 h followed by staining with DAPI for 10 min. The slices were imaged by confocal laser scanning microscope (CLSM, Zeiss Axio-Imager LSM-800).

For ROS staining, tumors were frozen at -20 °C, followed by fixing in acetone and washing with PBS. Then the tumor slices were successively incubated with DCFH-DA (20×10^{-6} M) for 1 h and DAPI for 10 min, respectively. The slices were imaged by confocal laser scanning microscope (CLSM, Zeiss Axio-Imager LSM-800).

For H&E staining, tumors were fixed in formaldehyde solution, followed by staining with hematoxylin and eosin (H&E). The slices were imaged by fluorescence microscope (Leica, DM4000M).

For TUNEL staining, tumors were fixed in formaldehyde solution, followed by staining with TdT-mediated dUTP Nick-End Labeling kit (TUNEL). The slices were imaged by confocal laser scanning microscope (CLSM, Zeiss Axio-Imager LSM-800).

In Vivo Long-Term Toxicity Assessment of PtCu₃-PEG: All animals were acclimated to the animal facility at least one week prior to experimental procedures. For long-time toxicity assessment, healthy female Balb/c mice were intravenously injected with 10 mg kg⁻¹ of PtCu₃-PEG for 1, 7, and 30 days, mice without administration were chosen as control. Blood samples were collected for blood routine and blood chemistry (liver and renal function) examination. In addition, vital organs including liver, spleen, kidney, heart, lung, stomach, and intestine were dissociated for H&E staining to observe morphological changes. Balb/c mice were purchased from Nanjing Sikerui Biological Technology Co. Ltd, and all animal experiments were carried out under the permission of the Soochow University Laboratory Animal Center.

Statistical Analysis: The experimental data were expressed quantitatively as mean \pm standard error of the mean (SEM), and analyzed by SPSS software (version 20.0; IBM Corp., Armonk, NY, USA) using independent *t*-test for comparison between two groups or one-way analysis of variance (ANOVA) for comparison among three or more groups. A statistical significance of $p < 0.05$ was selected, with (*) for $p < 0.05$, (**) for $p < 0.01$, and (***) for $p < 0.001$, respectively.

Supporting Information

Supporting Information is available from the Wiley Online Library or from the author.

Acknowledgements

This work was financially supported by National Science Foundation of China (Grant Nos. 81771978, 81627901, 81773653, and 51525203), grants from

National Basic Research Program of China (Grant Nos. 2015CB931802, 2016YFA0201200, and 2018YFA0208903), and Collaborative Innovation Center of Suzhou Nano Science and Technology, a Jiangsu Natural Science Fund for Distinguished Young Scholars (BK20170063). L.C. was supported by the Tang Scholar of Soochow University.

Conflict of Interest

The authors declare no conflict of interest.

Keywords

chemodynamic therapy, GSH depletion, nanozyme, PtCu₃ nanocages, sonodynamic therapy

Received: September 25, 2019

Published online:

- [1] R. L. Siegel, K. D. Miller, A. Jemal, *Ca-Cancer J. Clin.* **2016**, 66, 7.
- [2] M. Ferrari, *Nat. Rev. Cancer* **2005**, 5, 161.
- [3] Z. Guo, S. Zhu, Y. Yong, X. Zhang, X. Dong, J. Du, J. Xie, Q. Wang, Z. Gu, Y. Zhao, *Adv. Mater.* **2017**, 29, 12.
- [4] S. Li, Q. Jiang, S. Liu, Y. Zhang, Y. Tian, C. Song, J. Wang, Y. Zou, G. J. Anderson, J. Han, Y. Chang, Y. Liu, C. Zhang, L. Chen, G. Zhou, G. Nie, H. Yan, B. Ding, Y. Zhao, *Nat. Biotechnol.* **2018**, 36, 258.
- [5] Q. Liang, N. Bie, T. Yong, K. Tang, X. Shi, Z. Wei, H. Jia, X. Zhang, H. Zhao, W. Huang, L. Gan, B. Huang, X. Yang, *Nat. Biomed. Eng.* **2019**, 3, 729.
- [6] D. Ni, D. Jiang, C. J. Kutyreff, J. Lai, Y. Yan, T. E. Barnhart, B. Yu, H.-J. Im, L. Kang, S. Y. Cho, Z. Liu, P. Huang, J. W. Engle, W. Cai, *Nat. Commun.* **2018**, 9, 5421.
- [7] S. Yu, C. Wang, J. Yu, J. Q. Wang, Y. Lu, Y. Zhang, X. Zhang, Q. Hu, W. Sun, C. He, X. Chen, Z. Gu, *Adv. Mater.* **2018**, 30, 8.
- [8] Y. Liu, W. Zhen, Y. Wang, J. Liu, L. Jin, T. Zhang, S. Zhang, Y. Zhao, S. Song, C. Li, J. Zhu, Y. Yang, H. Zhang, *Angew. Chem., Int. Ed.* **2019**, 58, 2407.
- [9] S. S. Lucky, K. C. Soo, Y. Zhang, *Chem. Rev.* **2015**, 115, 1990.
- [10] W. Fan, P. Huang, X. Chen, *Chem. Soc. Rev.* **2016**, 45, 6488.
- [11] P. Huang, X. Qian, Y. Chen, L. Yu, H. Lin, L. Wane, Y. Zhu, J. Shi, *J. Am. Chem. Soc.* **2017**, 139, 1275.
- [12] A. Ma, H. Chen, Y. Cui, Z. Luo, R. Liang, Z. Wu, Z. Chen, T. Yin, J. Ni, M. Zheng, L. Cai, *Small* **2019**, 15, 1804028.
- [13] S. Mitragotri, *Nat. Rev. Drug Discovery* **2005**, 4, 255.
- [14] X. Pan, L. Bai, H. Wang, Q. Wu, H. Wang, S. Liu, B. Xu, X. Shi, H. Liu, *Adv. Mater.* **2018**, 30, 1800180.
- [15] X. Qian, Y. Zheng, Y. Chen, *Adv. Mater.* **2016**, 28, 8097.
- [16] D. Hanahan, R. A. Weinberg, *Cell* **2011**, 144, 646.
- [17] Y. Chen, D. Ye, M. Wu, H. Chen, L. Zhang, J. Shi, L. Wang, *Adv. Mater.* **2014**, 26, 7019.
- [18] W. Fan, W. Bu, B. Shen, Q. He, Z. Cui, Y. Liu, X. Zheng, K. Zhao, J. Shi, *Adv. Mater.* **2015**, 27, 4155.
- [19] J. Liu, W. Bu, J. Shi, *Chem. Rev.* **2017**, 117, 6160.
- [20] G. Song, C. Liang, H. Gong, M. Li, X. Zheng, L. Cheng, K. Yang, X. Jiang, Z. Liu, *Adv. Mater.* **2015**, 27, 6110.
- [21] Z. Tang, Y. Liu, M. He, W. Bu, *Angew. Chem., Int. Ed.* **2019**, 58, 946.
- [22] V. Catalano, A. Turdo, S. Di Franco, F. Dieli, M. Todaro, G. Stassi, *Semin. Cancer Biol.* **2013**, 23, 522.
- [23] Z. Dong, L. Feng, Y. Chao, Y. Hao, M. Chen, F. Gong, X. Han, R. Zhang, L. Cheng, Z. Liu, *Nano Lett.* **2019**, 19, 805.
- [24] F. Gong, L. Cheng, N. Yang, Q. Jin, L. Tian, M. Wang, Y. Li, Z. Liu, *Nano Lett.* **2018**, 18, 6037.
- [25] D. Trachootham, J. Alexandre, P. Huang, *Nat. Rev. Drug Discovery* **2009**, 8, 579.
- [26] F. Gong, L. Cheng, N. Yang, O. Betzer, L. Feng, Q. Zhou, Y. Li, R. Chen, R. Popovtzer, Z. Liu, *Adv. Mater.* **2019**, 31, 1900730.
- [27] E. Ju, K. Dong, Z. Chen, Z. Liu, C. Liu, Y. Huang, Z. Wang, F. Pu, J. Ren, X. Qu, *Angew. Chem., Int. Ed.* **2016**, 55, 11467.
- [28] C. Liu, D. Wang, S. Zhang, Y. Cheng, F. Yang, Y. Xing, T. Xu, H. Dong, X. Zhang, *ACS Nano* **2019**, 13, 4267.
- [29] A. Karakoti, S. Singh, J. M. Dowding, S. Seal, W. T. Self, *Chem. Soc. Rev.* **2010**, 39, 4422.
- [30] S. Yin, G. Song, Y. Yang, Y. Zhao, P. Wang, L. Zhu, X. Yin, X. Zhang, *Adv. Funct. Mater.* **2019**, 29, 1901417.
- [31] P. Wang, X. Wang, L. Ma, S. Sahi, L. Li, X. Wang, Q. Wang, Y. Chen, W. Chen, Q. Liu, *Part. Part. Syst. Character.* **2018**, 35, 1700378.
- [32] S. Wang, A. Riedinger, H. Li, C. Fu, H. Liu, L. Li, T. Liu, L. Tan, M. J. Barthel, G. Pugliese, F. De Donato, M. S. D'Abbusco, X. Meng, L. Manna, H. Meng, T. Pellegrino, *ACS Nano* **2015**, 9, 1788.
- [33] B. Ma, S. Wang, F. Liu, S. Zhang, J. Duan, Z. Li, Y. Kong, Y. Sang, H. Liu, W. Bu, L. Li, *J. Am. Chem. Soc.* **2019**, 141, 849.
- [34] B. Xia, H. Wu, X. Wang, X. Lou, *J. Am. Chem. Soc.* **2012**, 134, 13934.
- [35] R. Wu, Y. Chong, G. Fang, X. Jiang, Y. Pan, C. Chen, J. Yin, C. Ge, *Adv. Funct. Mater.* **2018**, 28, 1801484.
- [36] D. M. Kabtamu, G. Lin, Y. Chang, H. Chen, H. Huang, N. Hsu, Y. Chou, H. Wei, C. Wang, *RSC Adv.* **2018**, 8, 8537.
- [37] L. Cheng, W. He, H. Gong, C. Wang, Q. Chen, Z. Cheng, Z. Liu, *Adv. Funct. Mater.* **2013**, 23, 5893.
- [38] M. L. Bhaire, M. S. Khan, S. Pandey, G. Gedda, H. Wu, *RSC Adv.* **2017**, 7, 23607.
- [39] R. Chen, S. Pang, H. An, J. Zhu, S. Ye, Y. Gao, F. Fan, C. Li, *Nat. Energy* **2018**, 3, 655.
- [40] T. Zheng, T. Zhou, X. Feng, J. Shen, M. Zhang, Y. Sun, *ACS Appl. Mater. Interfaces* **2019**, 11, 31615.
- [41] H. Fan, G. Yan, Z. Zhao, X. Hu, W. Zhang, H. Liu, X. Fu, T. Fu, X.-B. Zhang, W. Tan, *Angew. Chem., Int. Ed.* **2016**, 55, 5477.
- [42] L. Lin, J. Song, L. Song, K. Ke, Y. Liu, Z. Zhou, Z. Shen, J. Li, Z. Yang, W. Tang, G. Niu, H. Yang, X. Chen, *Angew. Chem., Int. Ed.* **2018**, 57, 4902.
- [43] J. Yin, Y. Kwon, D. Kim, D. Lee, G. Kim, Y. Hu, J. H. Ryu, J. Yoon, *J. Am. Chem. Soc.* **2014**, 136, 5351.
- [44] X. Wang, X. Zhong, H. Lei, Y. Geng, Q. Zhao, F. Gong, Z. Yang, Z. Dong, Z. Liu, L. Cheng, *Chem. Mater.* **2019**, 31, 6174.
- [45] Kenry, Y. Duan, B. Liu, *Adv. Mater.* **2018**, 30, 1802394.